Title

Particles and Polymer Binder Interaction: A Controlling Factor in Lithium-Ion Electrode Performance

Permalink

https://escholarship.org/uc/item/32s0p8xc

Journal

Journal of The Electrochemical Society, 159(3)

ISSN

0013-4651

Authors

Liu, G
Zheng, H
Song, X
et al.

Publication Date

2012

DOI

10.1149/2.024203jes

Peer reviewed

Particles and Polymer Binder Interaction - A Controlling Factor in Lithium-ion Electrode Performance

Co-Authors

G. Liu[z], H. Zheng, X. Song, and V. S. Battaglia

Environmental Energy Technologies Division, Lawrence Berkeley National Laboratory,

Berkeley, CA 94720, USA

[z] Corresponding Author:

Gao Liu

Lawrence Berkeley National Laboratory

1 Cyclotron Rd., MS 70R108B

Berkeley, CA 94720

Office Phone: (510) 486-7207

Office Fax: (510) 486-7303

E-mail: Gliu@lbl.gov

Abstract

This paper investigates lithium-ion electrode laminates as polymer composites to explain their performance variation due to changes in formulation. There are three essential components in a positive electrode laminate: active material (AM) particles, acetylene black (AB) particles, and the polymer binder. The high filler content and discrete particle sizes make the electrode laminate a very unique polymer composite. This work introduces a model in which AB and AM particles compete for polymer binder, which forms fixed layers of polymer on their surfaces. This competition leads to the observed variations in electrode morphology and performance for different electrode formulations. The electronic conductivities of the cathode laminates were measured and compared to an effective conductivity model to probe the interaction among the three components and reveal the critical factors controlling electrode conductivity. The data and model results agree very well with each other. This developed model provides a theoretical guideline for optimization of electrode composition for most polymer binder-based Li-ion battery electrodes.

Introduction

Proper electrode design is critical to meeting both the energy and power performance requirements for any battery application.[1-4] Polymer binders and conductive additives used in Li-ion batteries, although not electrochemically active, are essential components in the electrodes, along with the active material (AM) that stores lithium ions. Conductive additives such as acetylene black (AB), a carbon black material composed of 40 nm-diameter particles, are used to provide the electronic conductivity from the current collector to the composite and surface conductivity to the micron-sized spherical AM particles. AB is an essential component for all cathodes due to its low cost and unique morphology.[14, 15] Primary AB particles fuse to form a branched structure, which allows for a fully percolated filler structure at much lower AB loading than would occur without the branching.[16, 17] This electrically conductive medium is needed to provide both long-range conductivity and short-range electron transport to the AM surface. A polymer binder such as polyvinylidine difluoride (PVDF) adheres the AB and AM particles together to form a continuous and robust electric conduction path to the current collector.

In designing an electrode, the AM content is preferentially high to maximize the energy density, but the inactive materials AB and PVDF are critical for electron transport and mechanical integrity, respectively. A typical cathode contains 90% AM, 4% AB, and 6% PVDF.[8] The AB content needs to be as low as the electrode design allows and still fulfill its function of providing electrical connection from the laminate to the current collector and amongst the AM particles throughout the laminate. The polymer content also needs to be as low as possible and still meet its design needs of binding the laminate to the current collector and holding all of particles together, even when the particles are experiencing volume changes during cycling. Therefore, the need to maximize energy density results in an electrode composite laminate that contains very low polymer content and a high concentration of filler particles. This composition requirement makes the electrode laminate a unique polymer composite as the filler content is extremely high compared to conventional polymer composites such as carbon black-filled rubber in the tire industry. Porosity of 25 to 45% in the final laminate is generated and maintained from the slurry coating process due to the high solid filler content. The porosity is critical for lithium-ion transport through electrolyte that fills the pores in the assembled cell. Another unique and

critical aspect of the composite is the inclusion of two size-discrete particles, AM and AB. Due to AB having a much larger specific surface area but much smaller percent composition than AM in the electrode, the total surface areas of the AM and AB particles are nearly equivalent.

It is well documented that the physical properties of polymers change when they are close to the surface of particles (Fig. 1).[17-20] Most thorough experimental and theoretical studies have been carried out in the carbon black-filled rubber systems, *i.e.* tires. Because of the dangling bonds on the surface of a solid particle, a polymer tends to chemically bond or physically absorb to form a 1 to 5 nm-thick bound polymer layer on the surface of the particle.[21] This layer of polymer cannot be re-dissolved back into solution. The polymer chains tend to stiffly align with the surface, so their physical properties change drastically. This bound polymer layer can interact with the polymer in the next layer to form a layer with reduced mobility called the immobilized polymer layer. Because of the reduced mobility of the polymer chains, both bound and immobilized layers tend to stay amorphous even if the bulk polymer is crystalline.[21] Free polymer domains do not appear in the composite until both bound and immobilized layers are formed on the surface of the particles. We can consider bound and immobilized layers together as a fixed polymer layer. The changes in glass transition temperature (T_g) and heat of fusion ($\mathit{\Delta H}$) of the polymer composites can be used to probe the content of the fixed polymer layer in a composite.[22, 23] Due to the high filler content of a typical electrode, almost all of the polymer is in the fixed state, leaving very limited free polymers. Therefore, changing the electrode composition, even by a few percent, has a significant consequence in power performance and cycling stability.

In order to decipher the relationship among the different components in the lithium-ion electrode, we have chosen $LiNi_{0.8}Co_{0.15}Al_{0.05}O_2$ with a defined particle size as the AM for this study and have systematically changed the compositions of AM, AB, and PVDF to demonstrate the performance changes in the electrode.   We use the bulk electronic conductivity of the electrode laminate as a probe to understand the effect of polymer binder distribution between the AB and AM. An effective conductivity model has been developed that takes into account the effect of fixed polymer layers on the particles.[24] The simulation demonstrates that the binder is not evenly distributed in the electrode; instead, it is preferentially distributed based on the surface area and

surface properties of the AB and AM. This preference in binder distribution is a significant factor in determining the electrode performance variation in lithium-ion cells.

Experimental

Materials. Battery-grade AB with an average particle size of 40 nm, BET surface area of 60 m^2/g, and a material density of 1.95 g/cm^3 was acquired from Denka Singapore Private Limited. PVDF KF1100 with a material density of 1.78 g/cm^3 and molecular weight of 280,000 Dalton was supplied by Kureha, Japan. Anhydrous N-methylpyrrolidone (NMP) with less than 50 ppm of water content was purchased from Aldrich Chemical Company. Active cathode material $LiNi_{0.8}Co_{0.15}Al_{0.05}O_2$, with a mean particle size of 10 μm, BET surface area of 0.78 m^2/g, and lattice density of 4.73 g/cm^3, was a gift from Toda, Japan. The manufacturer-suggested specific capacity is 173 mAh/g when cycled between 3 and 4.1 V. The active material was shipped under dry conditions from the manufacturer and stored in an argon (Ar) atmosphere glove box with an oxygen content less than 0.1 ppm and a dew point below -80ºC. The AB and PVDF powders were dried at 120ºC under 10^{-2} Torr dynamic vacuum for 12 to 24 hours on arrival. The dried AB and PVDF powder were stored in an Ar filled glove box.

The AB/PVDF mixtures were made by dissolving 5 g of PVDF in 95 g of anhydrous NMP. A given amount of AB was dispersed in the PVDF polymer solution to meet the desired AB:PVDF ratio. To ensure thorough mixing of the AB nanoparticles into the polymer solution, a Branson 450 sonicator equipped with a solid horn was used. The sonication power was set at 70%. A continuous sequence of 10 s pulses followed by 30 s rests was used. The sonic dispersion process took approximately 30 min. The properties of all AB/PVDF in NMP slurries were constant after 20 min of sonication. Slurries with active cathode material were made by adding the targeted amount of $LiNi_{0.8}Co_{0.15}Al_{0.05}O_2$ active material to the freshly pre-mixed AB/PVDF/NMP slurry. The cathode mixture was homogenized using a Polytron PT10-3S homogenizer at 3000 rpm for 15 min until a viscous, uniformly dispersed slurry was acquired. All of the mixing processes were performed in an Ar atmosphere glove box.

Electrode laminate casting. In order to understand the conductive behavior of the AB/PVDF composite system, different weight ratios of AB were dispersed in PVDF-NMP solutions and cast into thin films on glass plates. The film compositions ranged from 0.1:1 to 1:1 AB:PVDF weight ratios. Among the AB:PVDF ratios, 0.2:1, 0.4:1, 0.6:1 and 0.8:1 were chosen to mix with $LiNi_{0.8}Co_{0.15}Al_{0.05}O_2$ active material to fabricate electrodes. At 0.2:1 AB:PVDF ratio, electrode laminates were made of 98.8, 97.6, 95.2, 90.4, and 76% active material with the remainder being AB+PVDF. At 0.4:1 AB:PVDF ratio, electrode laminates were made of 97.6, 88.8 and 79% active material with the remainder being AB+PVDF. At 0.6:1 AB:PVDF ratio, electrode laminates were made of 96.8, 87.2, and 76% active material with the remainder being AB+PVDF. Finally, at 0.8:1 AB:PVDF ratio, electrode laminates were made of 96.4, 91, 82 and 73% active material with the remainder being AB+PVDF. Laminates were first dried under infrared lamps for 1 h until most of the NMP was evaporated and they appeared dried. They were further dried at 120°C under 10^{-2} Torr dynamic vacuum for 24 hrs. The film and laminate thicknesses were measured with a Mitutoyo micrometer with an accuracy of 1 μm. The typical thickness of the AB/PVDF films was *ca*. 20 μm with a density of *ca*. 1.2 g/cm^3. The typical thickness of the AB/PVDF/$LiNi_{0.8}Co_{0.15}Al_{0.05}O_2$ films was *ca*. 50 μm with a porosity of *ca*. 50% after drying.

Film imaging. The electrode surface morphology was imaged using a field-emission scanning electron microscope (FESEM) at 5 kV. EDX mapping of the electrode surface was performed on C, F, and Ni elements at 15 kV and a working distance of 8 mm from the sample. The bulk morphologies of 0.2:1 and 0.8:1 AB:PVDF composites were imaged by transmission electron microscopy (TEM), a JEOL 200CX microscope operating at 200 kV. An RMC Boeckeler PR XL ultramicrotome was used to prepare 50 nm thin sections for the TEM. Samples were embedded in low-viscosity Spurr's epoxy for added stability prior to sectioning. Films were microtomed at -100°C using a cryogenic attachment and a glass knife. After the samples were sectioned they were then carbon coated to help dissipate charge.

Four-point probe direct current (dc) testing. The conductivities of the AB/PVDF and AB/PVDF/$LiNi_{0.8}Co_{0.15}Al_{0.05}O_2$ films were measured using the four-point probe dc method. The dc conductivity measurement was performed using a Jandel equal-distance linear four-point probe apparatus with a Solatron 1286 Electrochemical Interface and a CorrWare software

package. A direct current is applied between the two outer probes; the voltage is registered between the two inner probes. The conductivities of AB/PVDF/ LiNi$_{0.8}$Co$_{0.15}$Al$_{0.05}$O$_2$ films were measured before and after compression.

Results and Discussion

This electron conduction function of AB can be separated into two ranges. The first is long-range conduction where electrons are carried from the current collector throughout the bulk of the electrode laminate. This conductivity is inversely proportional to the high frequency intercept of an ac impedance frequency sweep. For a well-constructed electrode, the long-range conductivity is seldom a performance limiting parameter. The second is a short-range conductivity that provides electrons to the surface of the AM to allow charge transfer at the interface. In lithium-ion cells, this interface impedance can dominate the cell impedance; therefore, it is a critical parameter in electrode design. In a three component AM/AB/PVDF system, the long-range conductivity is governed by the AB/PVDF domains. However, any change in the composition and distribution of the AB/PVDF domains also directly affects the short-range conductivity between AB and AM.[2] This study develops an effective conductivity model that closely approximates experimental measurements of the conductivities of AB/PVDF composites and AM/AB/PVDF composites of various compositions. This model can be used to probe the interaction among the three components to reveal the critical factors controlling electrode impedance.

AB/PVDF composites - morphology and conductivity

The hyper-branched AB particles have a very low percolation threshold when combined in a polymer composite. As low as 4%-wt. of AB in polymer was necessary to reach electronic percolation.[25] The electronic conductivity jumps to the high conductivity plateau at an AB:PVDF weight ratio of 0.2:1, indicating the formation of a continuous AB conductive network in the PVDF (Fig. 2).[16] The volume content is only 10% AB in the composite in this case. This is a

7

significant advantage for AB as a conductive additive, as a low AB content can be used to form the electrical network in the electrode. The schematic of Fig. 2A shows the AB forms a network of strands, and the rest of the PVDF aggregates in separate phases. Electrons pass through the AB network but not through the polymer phase.

In a traditional carbon black-filled rubber system, *e.g.* a tire, the filler particles are added to improve the mechanical strength of the composite. The mechanical strength of such a composite to resist tearing peaks once the filler network is fully formed.[26] As the filler contents is increased past this point, the polymer phase seen in Fig.2A,B is quickly lost as the polymer strongly binds with the filler particles, and the composite's mechanical strength is likewise forfeited.[26] Similarly, as the AB content increases in the AB/PVDF composites, the pure polymer phase shrinks due to the formation of the fixed polymer layer on the AB. At the higher AB content of 1:1 AB:PVDF, all of the PVDF is associated with fixed polymer layers on AB particles, as evidenced by the very depressed *ΔH* of the composite (Fig. S-1). Very little free polymer remains for inter-particle adhesion and particles become isolated. Therefore, the force to adhere the particles together is drastically diminished, as compared to the low AB content. This effect is reflected in the peaking of the conductivity from 0.2:1 to 0.8:1 and then its decline from 0.8:1 to 1:1 AB:PVDF (Fig. 2C,D).[2, 27] These conductivity trends can be expressed by eq. 1.1 from 0:1 to 0.5:1 AB:PVDF, and eq. 1.2 from 0.5:1 to 1:1 AB:PVDF. It is difficult to use one simple equation to express the conductivity for the entire range of compositions. (Note: The abscissa in Fig. 2D has been converted into vol/vol from w/w.)

AB/PVDF/AM composites - binder distribution

The amount of fixed polymer layer on filler particles is governed by filler surface area and the surface properties. In the case of a cathode electrode, there are two types of filler – AB and AM particles. Since AB and AM have very different surface chemistry and specific area, the PVDF binder forms different fixed layers on the surface of the AB and the AM. In the AB/PVDF composite, the PVDF forms a fixed layer on the surface of AB, and extra PVDF forms free domains (Fig. 3). When AM is introduced into the AB/PVDF, there will be fixed layers of PVDF

on both AM and AB, and the remaining PVDF forms free polymer domains (Fig. 3C). As Fig. 3A-C illustrates, the free polymer phase associated with the AB conductive network shrinks after the introduction of AM. Therefore, the conductivity of the AB/PVDF region will be different before and after the introduction of AM into the AB/PVDF composite.

The AM and AB compete for polymer binder in the electrode laminate. This competition influences the long-range electrode electronic conductivity as mentioned above. The lithium-ion transport resistance across the interface of the AM also varies as a result of PVDF binder rearrangement. The long-range conductivity and interface resistance become coordinated during the composition variation. The consequences of the competition are amplified by the unique composition requirement of the electrode, where high composition of AM and low composition of AB and PVDF are desirable for a high energy density electrode. Although the specific surface area of AM is smaller compared to that of the AB particle, the total amount of surface areas is equivalent between AB and AM (Fig. 3D). The desire to decrease inactive material content (AB, PVDF) may cause the binder amount to drop below the point where PVDF forms fixed layers on both the AB and AM. In this case, the fixed polymer layer forms on AB and AM based on a distribution factor d, leaving no free polymer among the particles (Fig. 3E).

Modeling the electronic conductivity

In this particular AB/AM/PVDF composite system, the electronic conductivity of the AM particles is low ($<10^{-3}$ S/cm),[9-11] so the electronic conductivity is provided solely by the AB/PVDF.[2, 9-11] The conductivity k of AB/PVDF is described by eq. 1, where c is the volume fraction of AB and b is the volume fraction of PVDF. The conductivity constant of a film of just AB and PVDF with no voids, k_o, was measured earlier and expressed by fitting eq. 1.1 and 1.2. When AM is introduced into the AB/PVDF system, the AM particles pull PVDF away from the AB/PVDF composite, causing the local AB to PVDF ratio to increase, resulting in a movement to the right on the abscissa of Fig. 2D. The change of AB/PVDF conductivity due to the PVDF binder redistribution is expressed by eq. 2, where b_a is the volume of binder attached to the AM. The conductivity equation was further refined to more accurately reflect that the space taken up

by both AM and porosity do not contribute to the electronic conductivity of the electrode laminate. In a practical electrode, the porosity is targeted at 30% to balance fast lithium-ion transport and high energy density. Therefore, to account for tortuosity of the current path through the AB/PVDF conductive medium that arises due to porosity, the effective conductivity equation includes the correction term $(c+b-b_a)^\rho$, where the volume of PVDF attached to the AM is subtracted and a tortuosity factor ρ is introduced (eq. 3). The tortuosity factor is difficult to experimentally determine, so it is left as a fitting parameter. In a composition where PVDF is abundant, such as Fig. 3D, the PVDF binder can form fixed layers on both AM and AB. Eq. 3 can be used to describe the effective conductivity of the electrode in this situation. However, when PVDF is limited, the fixed polymer layers cannot form completely on both AB and AM as in Fig. 3E. Therefore, there will be a distribution of PVDF between AB and AM. A PVDF distribution factor d is introduced in eq. 4 to approximate this situation; d is the volume ratio of fixed PVDF on AM to fixed PVDF on AB and is a fitting parameter in the model. When $d = 0$, all the PVDF is assumed fixed to the AB, whereas when $d = \infty$, all the PVDF is assumed fixed to the AM. When $d = 1$, the PVDF is assumed to be evenly distributed between AB and AM according to the surface area. The results indicate that 1.2 is the best fit for d for the entire set of experimental data. This suggests that the PVDF preferentially adheres to the AM. We do not know if this is a thermodynamic measure of preference or a metastable state that is a result of the order in which the materials were mixed. The parameters used in the modified effetive conductivity equation to calculate the electrode electrical conductivity is listed in Tab. I. The materials parameters used in the simulation are listed in Tab. II.

$k = k_o(c/b)$ eq. 1

$k_o(c/b) = 14.3(c/b)^2 + 0.12(c/b) – 0.11$ eq. 1.1

$k_o(c/b) = -119.3(c/b)^3 + 194.6(c/b)^2 - 89.9(c/b) + 14.6$ eq. 1.2

$k = k_o(c/(b-b_a))$ eq. 2

$k_e = (c+b-b_a)^\rho * k_0(c/(b-b_a))$ eq. 3

$k_e' = (c+b-d*b_a)^\rho * k_o(c/(b-d*b_a))$ eq. 4

The thickness of the fixed layers on the AB or AM is experimentally determined *via* studying the melting behavior of PVDF and its composites. Since the fixed layer of PVDF on particles has

reduced mobility, it does not effectively reorganize to participate in the melting and crystallization of a polymer composite. The depression of the heat of fusion (ΔH) can therefore be used to estimate the thickness of the fixed layer on particles. A detailed estimation can be found in the supplemental material section (Fig. S-1). The experimentally estimated thickness of fixed PVDF on AB is 9.5 nm and the thickness on AM is 32 nm, when excess PVDF is present. These thicknesses along with the average specific surface area of the particles are used to estimate the volume of the fixed binder to the particles. These fixed polymer layer thicknesses also support the notion that PVDF is preferentially adsorbed on the AM, as inferred from the best fit of the d parameter being larger than 1.

The effective conductivity expressions of eq. 3 and eq. 4 are used to fit the entire set of experimental data for the wide range of electrode compositions in Fig. 4. The conductivities were measured for four sets of different AB:PVDF compositions at 0.2:1, 0.4:1, 0.6:1, and 0.8:1, as mentioned earlier. Note that these AB:PVDF compositions span the entire high conductivity plateau of the AB/PVDF composite. At an AB:PVDF = 0.2:1, the conductivity is just above that of a fully formed conductive network and is considered to be on the upper conductivity plateau. This conductivity plateau corresponds to the formation of a 3-D network of AB structure in the composite. At AB:PVDF = 0.8:1, the conductivity peaks. As the AB content is further increased, the conductivity declines. Within each AB:PVDF composition, the active material content is varied from 64% to 98%. For designing high-energy electrodes, the AM content is typically targeted to be above 90%.

The experimental results show three distinct features of electronic conductivity behavior for the electrodes, and the model based on the polymer binder distribution theory captures all three:

1. Conductivities of the electrodes with different AB:PVDF ratios are very similar at high AM loading (e.g. > 95%) and begin to differ as the AM fraction decreases.
2. Conductivities of the electrodes increase to their AB:PVDF composite conductivity limits with decreasing AM content. The electrodes with lower AB:PVDF ratios tend to approach to their conductivity limit at a higher active material loading. For example, the conductivities of electrodes at AB:PVDF = 0.2:1 reach the conductivity plateau at 95% of

AM loading, whereas the conductivities of electrodes at AB:PVDF = 0.4:1 reach the conductivity plateau at about 90% AM loading.

3. The most conductive electrode with 78% - 95% AM content is obtained with the intermediate composition of AB:PVDF = 0.6:1 rather than the most conductive composition of AB:PVDF = 0.8:1.

All of the above behavior can be attributed to the binder distribution between the AM and AB particles. When the factor b_a is removed from eq. 3 and eq. 4, and everything else remains the same, the model does not fit the experimental data, and fails to account for the four features described above (Fig. S-2). A qualitative explanation of the effect of binder competition on the long-range electronic conductivity changes based on the modeling results can be described as follows:

1. The introduction of AM at a high fraction redistributes significant amounts of binder from AB onto the AM surfaces. This high AM loading (e.g., 95% and up) increases the particle surfaces for formation of fixed polymer layers and thereby reduces the amount of free binder available for connecting AB particles and results in conductivities that are in the far right regime of the AB/binder conductivity in Fig. 2D. The conductivities of all the electrodes are very similar despite the AB:PVDF composition since the composites are binder-limited.

2. When the AM content decreases, the AB surface starts to dominate, and AB/PVDF becomes the dominant composition. Therefore, the conductivities of the electrodes approach the pure AB/PVDF conductivities shown in Fig. 2D.

3. At the peak conductivity composition AB:PVDF = 0.8:1, the competition for binder by the AM causes a decrease of PVDF in the AB:PVDF conductive matrix and conductive paths are severed. Therefore, the conductivity declines in accordance with the curve in Fig. 2D. This accounts for the electrode conductivity dip at 80% to 95% of the AM content at AB:PVDF = 0.8:1.

This effective conductivity model described by eq. 1- 4 helps explain the varying conductivities of an electrode as a result of the binder distributions. This distribution has a dominant effect on the electrode impedance and hence the cell performance.

AB/PVDF/AM distribution and morphology in the electrode

The bulk electronic conductivity of the electrode and the simulation results are used to understand the binder distribution, which plays a critical role in the electrode microstructure and electrode performance. To visualize the distribution of all components in the composite electrode, schematic images are shown in Fig. 5 on the two extreme compositions of AB:PVDF for various AM contents, along with SEM images of the electrodes (Fig. S-3). Due to the high content of PVDF in AB:PVDF = 0.2:1, there will be free PVDF to cover the AM (Fig. 5C,D, S-3A-C). Based on the parameter fits of the model and SEM, there will be free PVDF polymer domains when the AM content is as high as 90.4% of the total electrode weight (Fig. S-3B). Therefore, the binder distribution satisfies the need for the fixed layers on both the AB and AM when the AM content is less than 90.4% (Fig. S-3B,C). When the AM content decreases in the electrode, the surface of AM becomes a small fraction of the overall surface area. Although the adhesion is better with more PVDF on AM, there will be higher lithium-ion transport resistance at the AM interface. Therefore, the interfacial impedance increases compared to higher AM loading. This impedance trend has been seen in the cell performance that we reported earlier.[2]

Due to the high AB content in electrodes with AB:PVDF = 0.8:1, the surface of AB dominates the composite structure. Based on the model, there is not enough binder to form fixed layers on both AB and AM particles when the AM content is above 73%. The AM competes with AB for the fixed polymer layer that is available. Therefore, AB tends to aggregate in the composite laminate (Fig. 5A,B, S-3D-F). The AB aggregation not only further diminishes adhesive properties of the electrode, but also causes limited contact area between the AB conductive matrix and AM surfaces. Since the AM particles do not have sufficient electronic conductivity, the limited contact area between the AM and AB aggregates reduces the overall area that is electrochemically active for lithium-ion insertion and removal. The reduction of electrochemically active area leads to an increase in area-specific impedance of the electrode.

However, when the AM content is low, the AM particles are surrounded by the AB/PVDF composite matrix (Fig. S-3F). In this case, the AM surface is well covered by the AB conductive network. The effective area for lithium-ion transport extends to the entire surface of the AM particles; therefore, the interface impedance (area specific to the electrode) drops dramatically. This impedance trend has been seen in the cell performance that we reported earlier.[2]

The uneven binder distribution on AB and AM can be detected by EDX (Fig. 6). In the electrode laminate, F atoms are part of the PVDF binder, but not AB and AM; the binder and AB both contain C atoms; and Ni is only contained within the AM. Although the PVDF content is the same (8%-wt.) in both cases of AB:PVDF = 0.2:1 and 0.8:1, there is free PVDF binder in AB:PVDF = 0.2:1 but all fixed PVDF in the 0.8:1 composition. F mappings show the PVDF is distributed more evenly in the electrode with AB:PVDF= 0.2:1 (Fig. 6C) containing free PVDF than that with AB:PVDF= 0.8:1 (Fig. 6G) containing all fixed PVDF. The AB is also distributed more evenly at high binder content of AB:PVDF = 0.2:1. At AB:PVDF = 0.8:1, the AM has taken away part of the fixed layer of PVDF from AB, causing AB to form aggregates. The AB aggregation leads to the distribution preference of the AM in the 0.8:1 composition.

Conclusions

The lithium-ion electrode laminate contains a very low polymer binder fraction and high concentrations of AM and AB filler particles. The high filler content and discrete particle sizes make the electrode laminate a very unique polymer composite. This work introduces the concept of fixed polymer layers on particles from the field of polymer composite engineering to understand variations in electrode performance. This has led to a new concept that AB and AM particles compete for polymer binder to form fixed layers of polymer on their surfaces. This is a fundamental reason for performance variation from small changes in electrode formulations.

An effective conductivity model was developed to simulate the electronic conductivity data from various cathode laminate compositions. This model included terms accounting for polymer binder distribution between the AB and AM. At high binder ratio (AB:PVDF = 0.2:1) and

increasing AM content, free polymer binder migrates partially to the AM surface to increase the AB:PVDF matrix conductivity. The free PVDF also allows for a more uniform distribution of AB, AM, and polymer binder within the electrode. However, when the AM content decreases, the free polymer binder exerts an impedance effect on the surface of the active material to slow down the lithium-ion transport at the interface. At low binder ratio (AB:PVDF = 0.8:1), the AB particles fix PVDF on their surface, and no free polymer is found. The addition of AM causes a competition for the fixed layer of binder. Stripping away PVDF from AB leads to the aggregation of the AB particles. This has two adverse effects on the electrode: it lowers the matrix conductivity and decreases the surface coverage of AM by AB particles, leading to high interfacial impedance. However, when AM content decreases, the AM particles are embedded in the conductive AB matrix while most of the binder is affixed to the AB materials. This serves to decrease the interfacial impedance of the electrode composite at low loading of active material. Therefore, a higher binder ratio can better accommodate high loading of AM and prevent stripping of binder from AB.

The polymer distribution on filler particles to form fixed layers is a universal phenomenon, and applicable to cathode and anode materials in the electrode system in general. However, the actual distribution factors between different particles depend on surface area and surface chemistry. Different types of materials or even different batches of similar materials may have very different surface chemistry. Therefore, electrode optimization is critical should optimum performance of a given material be required. Fortunately, in many situations, we are either after specific energy or power performance of a new material. A full-scale optimization is beyond the capability of a research lab with limited staff and instrumentation. This work and the developed model provide general guidelines for electrode optimization. In order to maximize the energy density of an electrode, the best composition to accommodate high content of AM is when the AB:PVDF ratio is low. The high binder content ensures good adhesion and acceptable matrix and interface impedance at very high AM loadings. Up to 95% of AM in an electrode can be accommodated. Should power performance be the primary concern, an easy composition would be high AB:PVDF and a low AM loading. This ensures that the AM particles are covered by AB particles, and that the binder is nearly completed affixed to the AB surface to avoid the impedance from free binder. For the lithium-ion manufacturer, after the composition is

optimized, the consistency of batch-to-batch material is very important to ensure reproducible performance. This consistency includes not only compositions but also particle size and surface area, as well as the surface chemistry of AM and AB.

Figure and Table Captions

Figure 1. The bulk polymer differentiates into three physical states when in contact with a particle surface. Bound polymer and immobilized polymer layers on a particle surface are defined as the fixed polymer layer.

Figure 2. AB/PVDF composite morphology and electronic conductivities. (A) A schematic drawing indicates the AB network in PVDF polymer. (B) The conductivity as a function of AB:PVDF weight ratio. (C) The conductivity as a function of AB:PVDF volume ratio.

Figure 3. Schematic of the formation of fixed polymer layers b_a and b_c on AM and AB, respectively, and the polymer binder redistribution when combining AM particles with the AB/PVDF composite. (A) AM particle. (B) AB/PVDF matrix. (C) Mixed AM/AB/PVDF. (D) There is enough polymer binder to form fixed layers on both AM and AB. (E) There is a deficiency of polymer binder to form the fixed layer on AM and AB.

Figure 4. The electronic conductivities of different compositions of the composite electrode (AM/AB/PVDF) based on four-point-probe measurements and modeling results. The open symbols are experimental results, and the filled symbols are modeling results with visual guidelines.

Figure 5. The schematics and SEM images of binder distributions between AB and AM at different electrode compositions. AB:PVDF = 0.8:1 at high AM loading (A) and low AM loading (B); AB:PVDF = 0.2:1 at high AM loading (C) and low AM loading (D). Scale bar: 20 μm.

Figure 6. SEM images (×500 magnification) and EDX mapping of electrode surface morphology at two different AB/PVDF compositions. At AB:PVDF = 0.2:1 and (AB+PVDF) 9.6% and 90.4% AM: SEM (A); carbon map (B); Fluorine map (C) and Nickel map (D). At AB:PVDF = 0.8:1 and (AB+PVDF) of 14.4% and AM of 85.6%: SEM (E); carbon map (F); Fluorine map (G) and Nickel map (H).

Table I. List of parameters used in the modified effective conductivity equation to calculate the electrode electrical conductivity.

Table II. List of material parameters used in the simulation.

References

1.   J. Christensen, V. Srinivasan and J. Newman, J. Electrochem. Soc. **153** (3), A560-A565 (2006).

2.   G. Liu, H. Zheng, S. Kim, Y. Deng, A. M. Minor, X. Song and V. S. Battaglia, J. Electrochem. Soc. **155** (12), A887-A892 (2008).

3.   G. Liu, H. Zheng, A. S. Simens, A. M. Minor, X. Song and V. S. Battaglia, J. Electrochem. Soc. **154** (12), A1129-A1134 (2007).

4.   H. H. Zheng, G. Liu, X. Y. Song, P. Ridgway, S. D. Xun and V. S. Battaglia, J. Electrochem. Soc. **157** (10), A1060-A1066 (2010).

5.   I. Belharouak, Y. K. Sun, J. Liu and K. Amine, J. Power Sources **123** (2), 247-252 (2003).

6.   A. N. Jansen, A. J. Kahaian, K. D. Kepler, P. A. Nelson, K. Amine, D. W. Dees, D. R. Vissers and M. M. Thackeray, J. Power Sources **81**, 902-905 (1999).

7.   R. B. Wright, J. P. Christophersen, C. G. Motloch, J. R. Belt, C. D. Ho, V. S. Battaglia, J. A. Barnes, T. Q. Duong and R. A. Sutula, J. Power Sources **119**, 865-869 (2003).

8.   R. B. Wright, C. G. Motloch, J. R. Belt, J. P. Christophersen, C. D. Ho, R. A. Richardson, I. Bloom, S. A. Jones, V. S. Battaglia, G. L. Henriksen, T. Unkelhaeuser, D. Ingersoll, H. L. Case, S. A. Rogers and R. A. Sutula, J. Power Sources **110** (2), 445-470 (2002).

9.   H. Tukamoto and A. R. West, J. Electrochem. Soc. **144** (9), 3164-3168 (1997).

10.   J. Wolfenstine, J. Power Sources **129** (2), 324-325 (2004).

11.   J. Jiang, K. W. Eberman, L. J. Krause and J. R. Dahn, J. Electrochem. Soc. **152** (9), A1874-A1878 (2005).

12.   N. Meethong, H. Y. S. Huang, W. C. Carter and Y. M. Chiang, Electrochem. Solid State Lett. **10** (5), A134-A138 (2007).

13.   B. Kang and G. Ceder, Nature **458** (7235), 190-193 (2009).

14.   Heidenre.Rd, W. M. Hess and L. L. Ban, J. Appl. Crystallogr. **1**, 1-& (1968).

15.   J. A. Ayala, W. M. Hess, F. D. Kistler and G. A. Joyce, Rubber Chem. Technol. **64** (1), 19-39 (1991).

16.   F. Carmona, Ann. Chim.-Sci. Mat. **13** (6), 395-443 (1988).

17.   E. M. Dannenberg, Rubber Chem. Technol. **59** (3), 512-524 (1986).

18.   C. M. Blow, Polymer **14** (7), 309-323 (1973).

19.   J. C. Kenny, V. J. McBrierty, Z. Rigbi and D. C. Douglass, Macromolecules **24** (2), 436-443 (1991).

20.   A. I. Medalia, J. Colloid Interface Sci. **32** (1), 115-& (1970).

21.   J. Y. Feng, J. X. Li and C. M. Chan, J. Appl. Polym. Sci. **85** (2), 358-365 (2002).

22.   I. L. Dubnikova, N. F. Kedrina, A. B. Solov'eva, V. A. Timofeeva, N. N. Rozhkova, N. A. Erina and T. S. Zarkhina, Polym. Sci. Ser. A **45** (3), 281-286 (2003).

23.   L. Priya and J. P. Jog, J. Polym. Sci. Pt. B-Polym. Phys. **40** (15), 1682-1689 (2002).

24.   J. Newman and K. E. Thomas-Alyea, *Electrochemical Systems*, 3rd ed. (John Wiley & Sons, Inc., Hoboken, New Jersey, 2004).

25.   N. Probst, European Rubber J. (1984).

26.   G. J. Lake and P. B. Lindley, J. Appl. Polym. Sci. **9** (4), 1233-& (1965).

27.   C. Zhang, X. S. Yi, S. Asai and M. Sumita, J. Mater. Sci. **35** (3), 673-683 (2000).

Particles and Polymer Binder Interaction - A Controlling Factor in Lithium-ion Electrode
Performance

G. Liu,[z] H. Zheng, X. Song, and V. S. Battaglia

Environmental Energy Technologies Division
Lawrence Berkeley National Laboratory
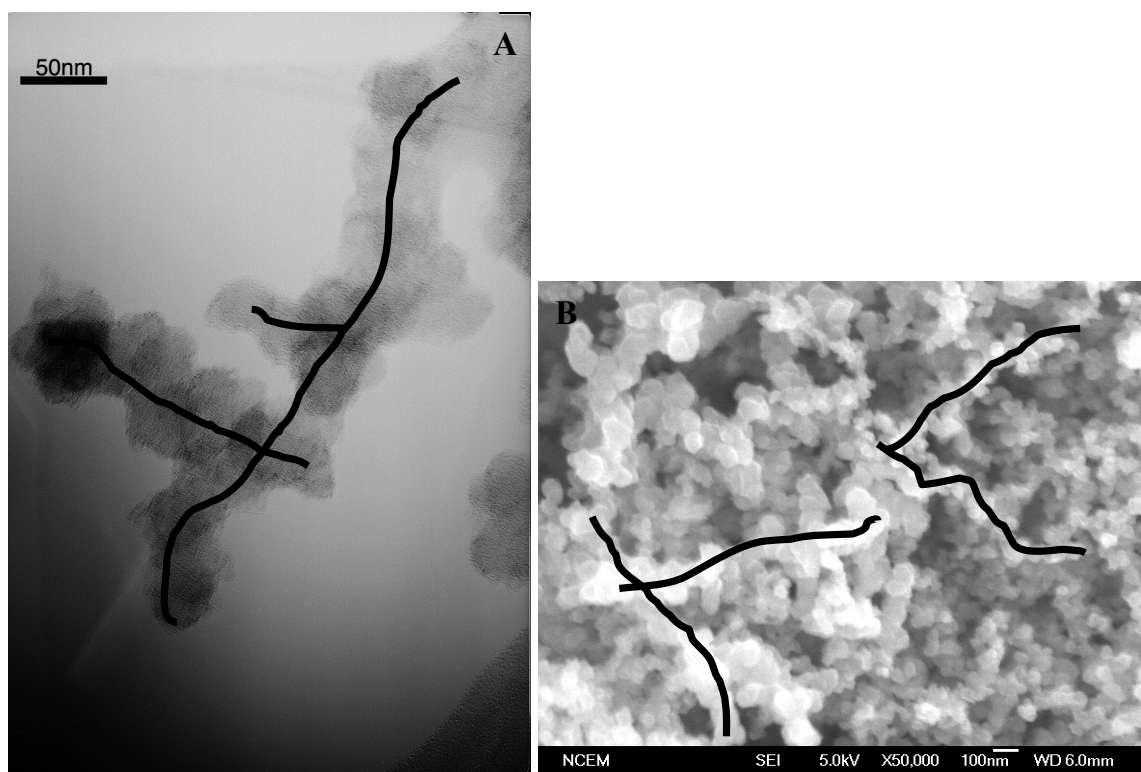Berkeley, CA 94720
USA

[z] E-mail: gliu@lbl.gov

Fig. S-1. A. TEM images of a fused AB primary particles to form structures. B. SEM images of
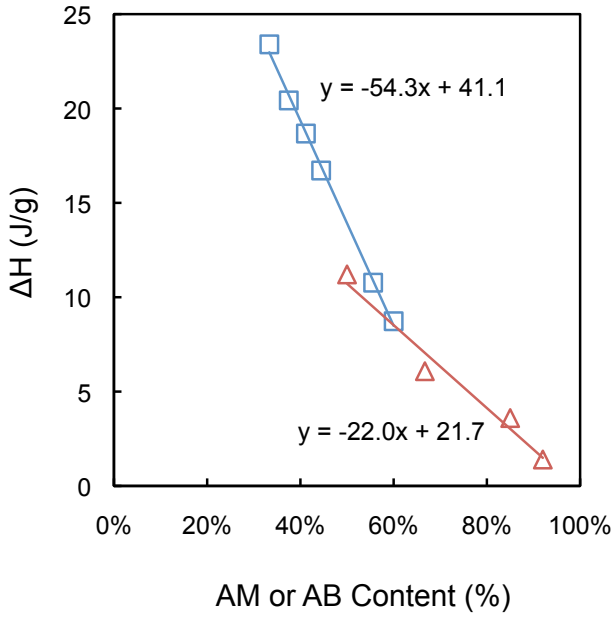fused AB primary particles. The solid lines are visual aid of the AB fused structures.

Fig. S-2. *ΔH* per PVDF vs. AB or AM content in the AB/PVDF (blue squares) and AM/PVDF (red triangles) series of composites. The lines and equations are a linear fit of each series.

Fig. S-2 shows *ΔH* per PVDF for the AB/PVDF (blue) or AM/PVDF (red) composites according to the fraction of particles to (particles+PVDF) ratios. One can also see a negative trend of *ΔH* with increase of the AB content in the mixture. This can be explained from the fact that the particle surface immobilizes the movement of the polymer chains, which are close to its surface. When the particle content increases, the surface area increases, and so does the polymer exposed to the surface of the particles. The kinetics for the fixed polymer layer to reorganize into the preferred structure to form crystalline polymer domains is very sluggish. Therefore, less and less polymer is able to participate in the crystallization process, causing the heat of fusion (*ΔH*) to decrease. Extrapolating the linear fit to *ΔH=0* for the AB and AM series leads to the fixed PVDF content (*eq. S-1*). When the surface area of the AB or AM is considered, the thickness of the fixed polymer layer can be determined (*eq. S-2*). The symbols and material parameters for the equations are listed in Tab. S-I.

$b_p = W_{PVDF}D/W_p$ *eq. S-1*
$t_p = b_p/S_P$ *eq. S-2*

Tab. S-I. List of symbols and material parameters for calculation of the fixed PVDF layer based on eq. S-1 and S-2.

Descriptions	Symbol	Origin
Volume of the fixed PVDF on particles	b_p	Calculated based on *eq. S-1*
Thickness of the fixed PVDF on particles	t_p	Calculated based on *eq. S-2*
Weight of fixed PVDF on particle surface	W_{PVDF}	Extrapolated to $\Delta H = 0$ based on Fig. S-1
Density of PVDF	$D = 1.78$ g/cm^3	Manufacturer provided
Weight of particles	W_p	Extrapolated to $\Delta H = 0$ based on Fig. S-1
Specific surface area of particles	S_p	Measured

AM content at *ΔH=0* from linear fit equation: 21.7/22 = 98.6%
Volume of the fixed PVDF layer on AM (b_a): 1.4×1.78/98.6 = 0.0253 cm^3 of PVDF per g of AM
Thickness of fixed PVDF on AM surface: $0.0253/(0.78×10^4)×10^7 = 32$ nm

AB content at *ΔH=0* from linear fit equation: 41.1/54.3 = 75.7%
Volume of the fixed PVDF layer on AB (b_c): 24.3×1.78/75.7 = 0.57 cm^3 of PVDF per g of AB
Thickness of fixed PVDF on AB surface: $0.57/(60×10^4)×10^7 = 9.5$ nm

Tab. S-II. Measured porosities of the laminates.

AB:PVDF groups	Active material content (%)	Porosities (%)
0.2:1	98.8	45.2
	97.6	47.5
	96.4	50.9
	95.2	45.6
	90.4	47.5
	88.0	46.1
	82.0	44.2
	76.0	41.7
	64.0	33.2
0.4:1	97.2	48.7

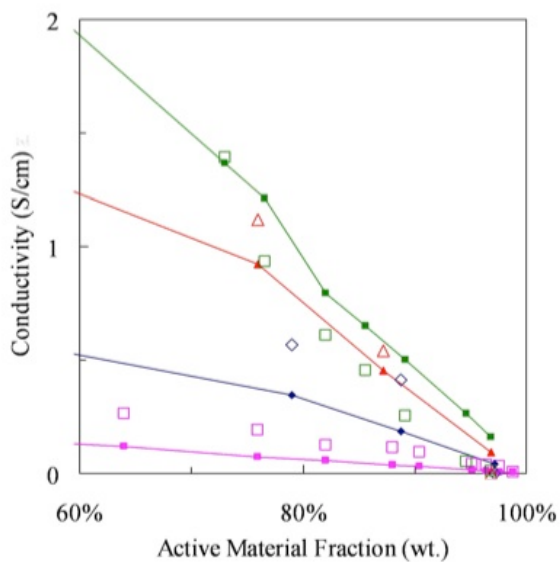|		
	88.8	43.5
	79.0	41.1
0.6:1	96.8	54.9
	87.2	47.4
	76.0	39.8
0.8:1	96.8	49.8
	94.6	52.5
	89.2	54.3
	85.6	54.8
	82.0	54.8
	76.6	49.5
	73.3	45.8

Fig. S-3. The electronic conductivities of different compositions of the composite electrode (AM/AB/PVDF) based on four-point-probe measurements and modeling results. The open symbols are experimental results, and the filled symbols are modeling results when b_a factors are removed from the equations.
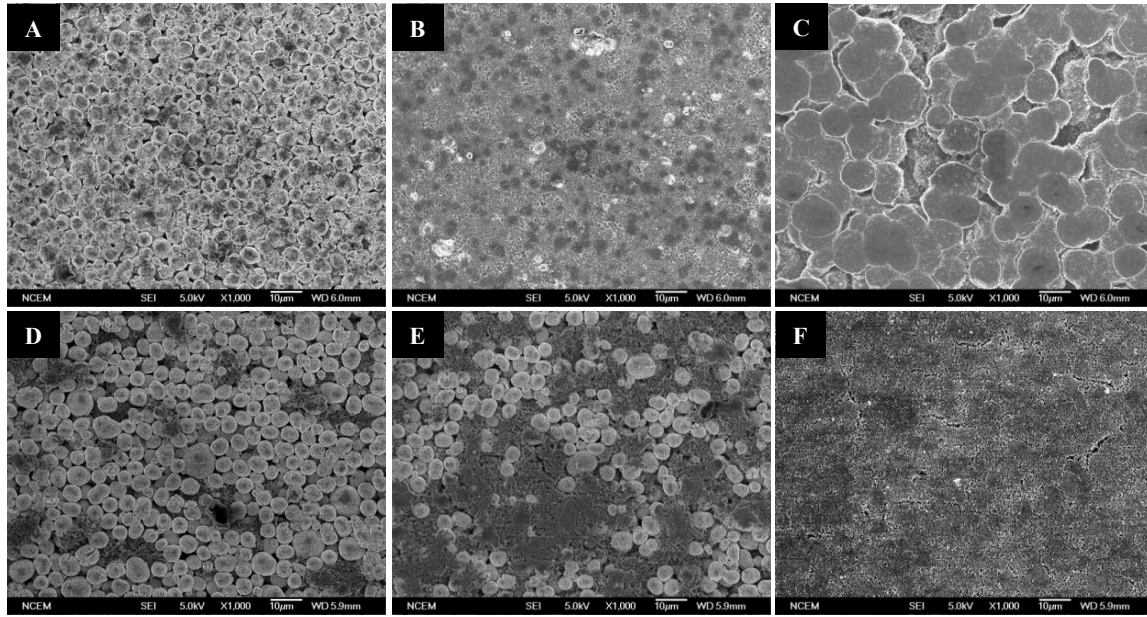
Fig. S-4. SEM images of positive electrode surface morphology at different AM/AB/PVDF compositions. At AB:PVDF = 0.2:1, (AB+PVDF) content of 1.2% (A); 9.6% (B) and 24% (C). At AB:PVDF = 0.8:1, (AB+PVDF) content of 4.5% (D); 18% (E) and 27% (F).